Functional properties and toxin pharmacology of a dorsal root ganglion sodium channel viewed through its voltage sensors

Frank Bosmans,[1] Michelino Puopolo,[2] Marie-France Martin-Eauclaire,[3] Bruce P. Bean,[2] and Kenton J. Swartz[1]

[1]Molecular Physiology and Biophysics Section, Porter Neuroscience Research Center, National Institute of Neurological Disorders and Stroke, National Institutes of Health, Bethesda, MD 20892
[2]Department of Neurobiology, Harvard Medical School, Boston, MA 02115
[3]Centre National de la Recherche Scientifique, UMR 6132, CRN2M, Institut Jean Roche, Université de la Méditerranée, 13916 Marseille Cedex 20, France

The voltage-activated sodium (Nav) channel Nav1.9 is expressed in dorsal root ganglion (DRG) neurons where it is believed to play an important role in nociception. Progress in revealing the functional properties and pharmacological sensitivities of this non-canonical Nav channel has been slow because attempts to express this channel in a heterologous expression system have been unsuccessful. Here, we use a protein engineering approach to dissect the contributions of the four Nav1.9 voltage sensors to channel function and pharmacology. We define individual S3b–S4 paddle motifs within each voltage sensor, and show that they can sense changes in membrane voltage and drive voltage sensor activation when transplanted into voltage-activated potassium channels. We also find that the paddle motifs in Nav1.9 are targeted by animal toxins, and that these toxins alter Nav1.9-mediated currents in DRG neurons. Our results demonstrate that slowly activating and inactivating Nav1.9 channels have functional and pharmacological properties in common with canonical Nav channels, but also show distinctive pharmacological sensitivities that can potentially be exploited for developing novel treatments for pain.

The Journal of General Physiology

INTRODUCTION

Neurons throughout the nervous system use voltage-activated sodium (Nav) channels to rapidly propagate electrical signals, often over long distances (Hille, 2001). In specialized peripheral neurons in the dorsal root ganglion (DRG), Nav channels are crucial for transmitting nociceptive sensory information to the central nervous system (Baker and Wood, 2001; Dib-Hajj et al., 2010). Of the nine Nav channel isoforms identified in humans (Nav1.1–Nav1.9), three are primarily expressed in the peripheral nervous system: Nav1.7 is present in both sensory and sympathetic neurons, whereas Nav1.8 and Nav1.9 are mainly found within small-diameter (≤27-µm) neurons in DRG and trigeminal ganglia (Catterall, 2000). Because of their strategic expression in sensory neurons, these three Nav channel isoforms have been the subject of studies aimed at elucidating their roles in nociception (Akopian et al., 1999; Dib-Hajj et al., 2002, 2010; Nassar et al., 2004; Priest et al., 2005; Amaya et al., 2006; Cox et al., 2006; Fang et al., 2006; Fertleman et al., 2006; Zimmermann et al., 2007; Leo et al., 2010).

Nav1.9 is a particularly interesting sensory neuron-specific channel because it has the most divergent amino acid sequence among all Nav channel isoforms (Hille, 2001), and it has uncharacteristically slow activation and inactivation kinetics in DRG neurons (Cummins et al., 1999; Maruyama et al., 2004; Priest et al., 2005; Maingret et al., 2008; Ostman et al., 2008). Compared with canonical Nav channels (Nav1.1–Nav1.7), the functional and pharmacological properties of this non-canonical channel are relatively unexplored (Dib-Hajj et al., 2002), in part because it cannot be reliably studied in heterologous expression systems. Indeed, we have tried to express Nav1.9 in *Xenopus laevis* oocytes and various mammalian cell lines along with an array of auxiliary β subunits and regulatory proteins, but have not been able to record the activity of functional channels. In the present study, we circumvent this obstacle by transplanting specific regions from the putative voltage sensors of both the human (h) and rat (r) Nav1.9 orthologues into voltage-activated potassium (Kv) channels and studying their response to changes in membrane voltage and exploring whether they interact with protein toxins from venomous organisms. To test whether the

Correspondence to Frank Bosmans: Frank.Bosmans@nih.gov; or Kenton Swartz: Kenton.Swartz@nih.gov

M. Puopolo's present address is Dept. of Anesthesiology, Stony Brook Medical Center, Stony Brook, NY 11794.

Abbreviations used in this paper: DRG, dorsal root ganglion; Kv, voltage-activated potassium; Nav, voltage-activated sodium; TTX, tetrodotoxin.

The Rockefeller University Press $30.00
J. Gen. Physiol. Vol. 138 No. 1 59–72
www.jgp.org/cgi/doi/10.1085/jgp.201110614

native Nav1.9 channel is sensitive to toxins identified using this approach, we examined the pharmacological sensitivity of Nav1.9-mediated currents in rat DRG neurons. Our results suggest that Nav1.9 channels possess functional voltage sensors that interact with scorpion and tarantula toxins, features that are shared with canonical Nav channel isoforms. We also demonstrate that the voltage sensor pharmacology of these channels differs from other Nav channels.

MATERIALS AND METHODS

Channel and chimera constructs

Chimeras and point mutations were generated using sequential PCR with Kv2.1Δ7 (Frech et al., 1989; Swartz and MacKinnon, 1997a), Kv1.3 (Stühmer et al., 1989), rNav1.8 (Akopian et al., 1996), or hNav1.9 (Blum et al., 2002) as templates. Kv1.3, rNav1.8, and hNav1.9 clones were provided by C. Deutsch (University of Pennsylvania, Philadelphia, PA), J.N. Wood (University College London, London, England, UK), and R. Blum (LMU, Munich, Germany), respectively. β1 was provided by L.L. Isom (University of Michigan, Ann Arbor, MI). rNav1.9/Kv2.1 chimeras were constructed using synthetic DNA coding for the S3b–S4 paddle motifs in each of the four rNav1.9 voltage sensors (Integrated DNA Technologies). The Kv2.1Δ7 construct contains seven point mutations in the outer vestibule (Swartz and MacKinnon, 1997a), rendering the channel sensitive to agitoxin-2, a pore-blocking toxin from scorpion venom (Garcia et al., 1994). The DNA sequence of all constructs and mutants was confirmed by automated DNA sequencing, and cRNA was synthesized using T7/SP6 polymerase (mMessage mMachine kit; Invitrogen) after linearizing the DNA with appropriate restriction enzymes.

Spider and scorpion toxin purification

AahI and AaHII from *Androctonus australis* hector venom, TsVII from *Tityus serrulatus* venom (provided by C. Diniz, Centro de Pesquisa e Desenvolvimento, Belo Horizonte, Brazil), BotIII from *Buthus occitanus* tunetanus venom, BomIV from *Buthus occitanus* mardochei venom, and CssIV and CssVI from *Centruroides suffuses* suffuses venom were purified as described previously (Martin et al., 1987a,b; Céard et al., 1992; Cestèle et al., 1999). Synthetic ProTx-I was acquired from Peptides International, and purified PaurTx3 was acquired from Alomone Laboratories. ProTx-II, GxTx-1E, and Ap-B were provided by M.M. Smith (Merck, Rahway, NJ), J.I. Kim (Gwangju Institute of Science and Technology, Gwangju, Korea), and K.M. Blumenthal (SUNY Buffalo, Buffalo, NY), respectively. Hanatoxin was purified from *Grammostola spatulata* venom (Spider Pharm Inc.) as described previously (Swartz and MacKinnon, 1995). SGTx1 and VsTx1 were synthesized using solid-phase chemical methods and were folded and purified as described previously (Lee et al., 2004; Jung et al., 2005). GrTx-SIA, SNX-482, and ATX-II were acquired from Sigma-Aldrich. Toxins were kept at −20°C. Before experiments, toxin aliquots were dissolved in appropriate solutions containing 0.1% BSA (or 1% BSA in the case of TsVII).

Two-electrode voltage clamp recording from *Xenopus* oocytes

Channel constructs and rNav1.8/β1 were expressed in *Xenopus* oocytes and studied after 1–4-d incubation after cRNA injection (incubated at 17°C in 96 mM NaCl, 2 mM KCl, 5 mM HEPES, 1 mM $MgCl_2$, 1.8 mM $CaCl_2$, and 50 µg/ml gentamycin, pH 7.6 with NaOH) using two-electrode voltage clamp recording techniques (OC-725C; Warner Instruments) with a 150-µl recording chamber. Data were filtered at 3 kHz and digitized at 20 kHz using pClamp software (Molecular Devices). Microelectrode resistances were 0.1–1 MΩ when filled with 3 M KCl. For most Kv channel experiments, the external recording solution contained: 50 mM KCl, 50 mM NaCl, 5 mM HEPES, 1 mM $MgCl_2$, and 0.3 mM $CaCl_2$, pH 7.6 with NaOH. For Nav channel experiments, the external recording solution contained 96 mM NaCl, 2 mM KCl, 5 mM HEPES, 1 mM $MgCl_2$, and 1.8 mM $CaCl_2$, pH 7.6 with NaOH. For Nav channel experiments, oocytes were coinjected with the β1 subunit (Isom et al., 1992) in a 1:5 molar ratio. All experiments were performed at room temperature (~22°C). Leak and background conductances, identified by blocking the channel with agitoxin-2, have been subtracted for all of the Kv channel currents shown. The rNav1.8 isoform was rendered tetrodotoxin (TTX) sensitive by introducing the S356F mutation (Sivilotti et al., 1997) so that the toxin could be used to isolate Nav channel currents.

Analysis of channel activity and toxin–channel interactions

Voltage–activation relationships were obtained by measuring tail currents for Kv channels or steady-state currents and calculating conductance for Nav channels, and a single Boltzmann function was fitted to the data according to: $I/I_{max} = (1 + e^{-zF(V - V_{1/2})/RT})^{-1}$, where I/I_{max} is the normalized tail current amplitude, z is the equivalent charge, $V_{1/2}$ is the half-activation voltage, F is Faraday's constant, R is the gas constant, and T is temperature in Kelvin. Occupancy of closed or resting channels by toxins was examined using negative holding voltages where open probability was very low, and the fraction of unbound channels (Fu) was estimated using depolarizations that are too weak to open toxin-bound channels, as described previously (Swartz and MacKinnon, 1997a,b; Li-Smerin and Swartz, 2000; Phillips et al., 2005). After the addition of the toxin to the recording chamber, the equilibration between the toxin and the channel was monitored using weak depolarizations elicited at 5–10-s intervals. For all channels, we recorded voltage–activation relationships in the absence and presence of toxin. The apparent equilibrium dissociation constant (K_d) for rNav1.8 was calculated according to $K_d = ((1/(1 - Fu^{1/3})) - 1)[Toxin]$, assuming three independent toxin-binding sites per channel, with single occupancy being sufficient to inhibit opening in response to weak depolarizations. Offline data analysis was performed using Clampfit (Molecular Devices), Origin 7.5 (OriginLab), and Microsoft Solver (Microsoft Excel).

DRG preparation

Isolated DRG neurons were prepared from rats (postnatal day 20–30). Animals were anesthetized with isoflurane and decapitated. Segments of the spinal cord (thoracic and lumbar segments) were removed and placed in a cold Ca^{2+}, Mg^{2+}-free Hanks' solution containing (in mM): 137 NaCl, 5.3 KCl, 0.33 Na_2HPO_4, 0.44 KH_2PO_4, 5 HEPES, and 5.5 glucose, pH 7.4 with NaOH. The bone surrounding the spinal cord was removed, and dorsal root ganglia were exposed and pulled out. After removing the roots, ganglia were chopped in half and incubated for 20 min at 34°C in Ca^{2+}, Mg^{2+}-free Hanks' solution containing 20 U/ml papain (Worthington Biochemical Corporation) and 5 mM cysteine. Ganglia were washed and incubated for 20 min at 34°C in Ca^{2+}, Mg^{2+}-free Hanks' solution containing 3 mg/ml collagenase (type I; Sigma-Aldrich) and 4 mg/ml Dispase II (Roche). Ganglia were then placed in Leibovitz's L-15 medium (Invitrogen) supplemented with 10% fetal calf serum, 5 mM HEPES, and 50 ng/ml NGF (Invitrogen). Individual cells were dispersed by mechanical trituration using a fire-polished Pasteur pipette and plated on glass coverslips treated with 50 µg/ml poly-D-lysine. Cells were incubated at 34°C in a controlled atmosphere with 5% CO_2 for 3 h, after which cells were stored at 4°C and used within 24 h (Blair and Bean, 2002).

DRG patch clamp recording

Experiments were performed on small DRG neurons with a diameter of ≤30 µm. Whole cell recordings were made with a Multiclamp 700B amplifier (Molecular Devices). Patch pipettes were pulled from borosilicate glass (100 µl microcapillaries; VWR International) using a P97 puller (Sutter Instrument). The resistance of the patch pipette was 1.8–2.5 MΩ when filled with the standard internal solution containing (in mM): 67.5 CsCl, 67.5 CsF, 10 NaCl, 2 $MgCl_2$, 10 EGTA, 10 HEPES, 14 Tris-creatine PO_4, 4 Mg-ATP, and 0.3 Na-GTP, pH 7.2 with CsOH. Patch pipettes were wrapped with Parafilm (Pechiney Plastic Packaging) to reduce pipette capacitance. Seals and whole cell configuration were established in a modified Tyrode's solution containing (in mM): 151 NaCl, 2 $BaCl_2$, 0.03 $CdCl_2$, 10 HEPES, and 13 glucose, pH 7.4 with NaOH. The inclusion of 30 µM Cd^{2+} served to inhibit calcium channel current without significantly blocking Nav1.8 or Nav1.9-mediated sodium current (Blair and Bean, 2002; Coste et al., 2007). After the whole cell configuration was established, the cell was lifted off the coverslip surface and placed in front of an array of quartz capillary tubes (internal diameter, 325 µm) to allow fast changes of external solution. External recording solution was a modified Tyrode's solution containing 300 nM TTX to block TTX-sensitive sodium current. In whole cell mode, the series resistance was ≤10 MΩ and was compensated up to 80%. Currents were filtered at 10 kHz and digitized at 50 kHz.

Online supplemental material

Fig. S1 defines the paddle motifs in Nav1.9 and rNav1.8. Fig. S2 shows an alignment of the paddle motif sequences in the four domains of the Nav channel family. Fig. S3 compares the gating properties of hNav1.9/Kv2.1 and hNav1.9/Kv1.3 constructs with rNav1.2a/Kv2.1 and rNav1.4/Kv1.3 chimeras. Fig. S4 describes the tail current voltage–activation relationships resulting from the transfer of the voltage sensor paddle motifs from hNav1.9 to Kv1.3. Fig. S5 illustrates the sensitivity of hNav1.9/Kv2.1 constructs to extracellular toxins. Fig. S6 reports the sensitivity of hNav1.9/Kv2.1 and hNav1.9/Kv1.3 DIII constructs to ProTx-I and HaTx. Fig. S7 compares the toxin sensitivities of hNav1.9/Kv2.1 and rNav1.2a/Kv2.1 constructs. Fig. S8 shows the tail current voltage–activation relationships resulting from the transfer of the voltage sensor paddle motifs from rNav1.8 to Kv2.1. Table S1 summarizes the gating properties of Kv2.1 and Kv1.3 channels containing paddle motifs from Nav1.8 and Nav1.9. The supplemental material is available at http://www.jgp.org/cgi/content/full/jgp.201110614/DC1.

RESULTS

Transfer of hNav1.9 paddle motifs into Kv channels

All Nav channels consist of four connected domains (I–IV) (Catterall, 2000), each resembling a single subunit of a Kv channel (Long et al., 2007). These highly similar domains each contain an S1–S4 voltage-sensing domain and contribute S5–S6 segments to forming a central Na^+-conducting pore. Studies on the related voltage sensors in Kv channels have identified an S3b–S4 helix-turn-helix motif, the voltage sensor paddle, which moves at the protein–lipid interface and drives activation of the voltage sensors and opening of the pore (Jiang et al., 2003a,b; Ruta et al., 2005; Alabi et al., 2007; Long et al., 2007; Chakrapani et al., 2008). Recently, it was shown that paddle motifs are also an integral part of the voltage sensors in rNav1.2a and rNav1.4 (Bosmans et al., 2008). As in Kv channels (Alabi et al., 2007), the paddle motifs in these two Nav channel isoforms are essential for voltage sensor activation and forming toxin receptor sites (Bosmans et al., 2008).

Our initial goal was to establish whether the four S1–S4 domains in hNav1.9 channels can sense changes in membrane voltage by identifying paddle motifs that perform similar functions as in Kv channels and canonical Nav channels. To this end, we asked whether we could transplant specific S3b–S4 regions from the putative voltage-sensing domains of hNav1.9 into homotetrameric Kv2.1 channels without disrupting channel function (Fig. 1 A). Although this approach successfully identified paddle motifs in rNav1.2a and rNav1.4, the amino acid sequence of the non-canonical hNav1.9 channel differs substantially, particularly in the S3b–S4 regions (Figs. S1 A and S2). For the domains I, II, and IV of hNav1.9, generating functional paddle chimeras (Fig. 1, B and C) was relatively straightforward using previously described boundaries for the paddle motif (Alabi et al., 2007; Bosmans et al., 2008). In the case of the domain III paddle motif, we were only able to record ionic currents when the N-terminal half of S3b was not transferred (Figs. 1, B and C, and S1 A). The pharmacological sensitivity of this chimera (see below) must therefore be considered cautiously because a substantial portion of the S3b helix from Kv2.1 remains intact and in some cases contains crucial determinants of toxin binding (Swartz and MacKinnon, 1997b; Li-Smerin and Swartz, 2000; Phillips et al., 2005; Alabi et al., 2007; Bosmans et al., 2008). However, the transferred region in all of the functional chimeras contains the essential basic residues that contribute to gating charge movement in Kv channels (Aggarwal and MacKinnon, 1996; Seoh et al., 1996), suggesting that each of the four putative voltage sensors in hNav1.9 contains S3b–S4 paddle motifs that are capable of sensing changes in membrane voltage.

Examination of the G-V relations for the hNav1.9/Kv2.1 paddle chimeras reveals that the paddle motifs from different domains have distinct effects on the gating properties of Kv2.1. The midpoints (and slopes) of the G-V relations for the four paddle chimeras are −10 mV (1.5), 1 mV (2.3), 19 mV (1.9), and 29 mV (1.6) for the domain II, I, III, and IV constructs, respectively (Fig. 1 C and Table S1). Although the same relative order of midpoints is observed when the domain II, III, and IV paddles are transplanted into Kv1.3, the domain I constructs are dramatically different between the two host Kv channels (Fig. S4). This comparison reveals that the gating properties of the chimeras are determined by the transplanted hNav1.9 paddle motifs and by the host Kv channel. These observations are not surprising given the complexity of gating transitions observed in Kv channels and the involvement of distinct regions (e.g., voltage sensors, S4–S5 linker, and S6 gate) within the channel (Bezanilla et al., 1994; Hoshi et al., 1994; Stefani

et al., 1994; Zagotta et al., 1994a,b; Schoppa and Sigworth, 1998a,b,c; Smith-Maxwell et al., 1998a,b; Ledwell and Aldrich, 1999; Sukhareva et al., 2003; del Camino et al., 2005; Pathak et al., 2005; Swartz, 2008).

Kinetics of hNav1.9 paddle chimeras

Previous studies on rNav1.4 and hNav1.5 reveal that the voltage sensors in domains I–III move rapidly in response to changes in membrane voltage to trigger channel opening, whereas the response of the domain IV voltage sensor is slower and plays a crucial role in channel inactivation (Sheets et al., 1999; Horn et al., 2000; Chanda and Bezanilla, 2002; Campos et al., 2008). Interestingly, domain IV paddle motifs from rNav1.2a and rNav1.4 slow opening when transplanted into Kv channels, suggesting that the domain IV paddle motif determines the slower kinetics of voltage sensor activation (Bosmans et al., 2008). To explore whether domain IV serves a similar role in hNav1.9, we measured the kinetics of activation and deactivation of the four hNav1.9 paddle constructs in response to membrane depolarization and repolarization, respectively (Fig. 2 A). In contrast to what is observed in previously studied chimeras containing paddle motifs from rNav1.2a and rNav1.4, the kinetics observed for the domain IV construct of hNav1.9 does not stand out compared with the other domains, and there are considerable differences when the hNav1.9 paddles are transplanted into Kv2.1 or Kv1.3 backgrounds (Figs. 2 and S3). However, one consistent trend is that constructs containing the paddle motifs from domains II, III, and IV exhibit relatively slow kinetics, comparable to what is observed for domain IV from rNav1.2a and rNav1.4 (Fig. S3). This observation raises the intriguing possibility that the slow kinetics of Nav1.9 gating observed in rat DRG neurons (Cummins et al., 1999; Maruyama et al., 2004; Baker, 2005; Priest et al., 2005; Coste et al., 2007; Ostman et al., 2008; Copel et al., 2009) may result from slow activation of its voltage sensors rather than slow subsequent transitions (e.g., opening or inactivation).

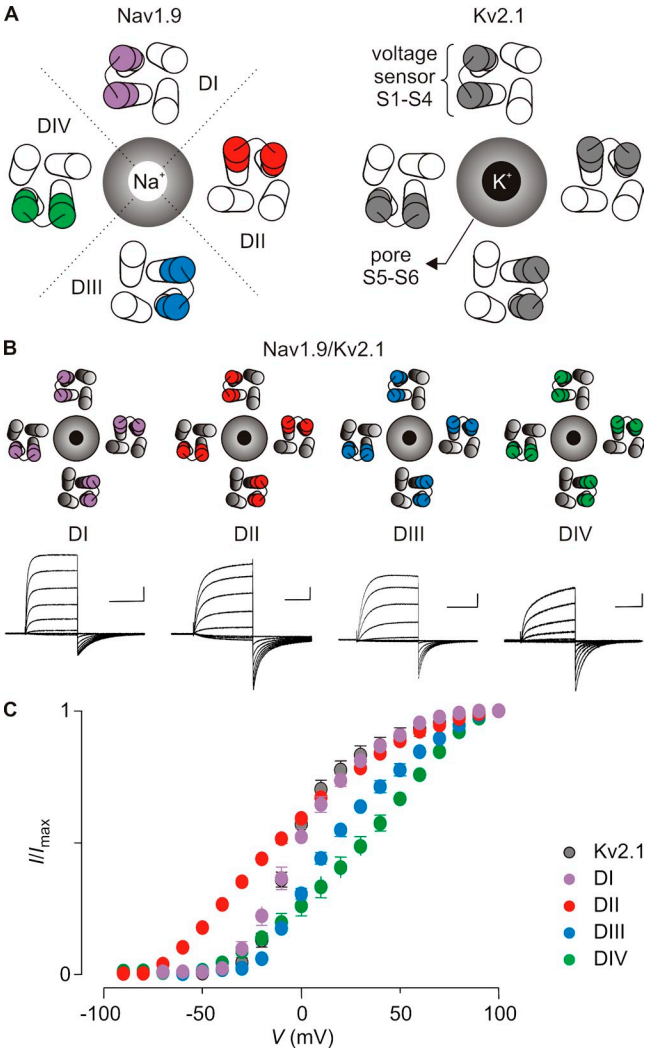

Figure 1. Transfer of the voltage sensor paddle motifs from hNav1.9 to Kv2.1. (A) Cartoon representing a top view of Nav1.9 (left) and Kv2.1 (right). The central Na^+- or K^+-selective pore is surrounded by the four voltage sensors of the four domains (DI–DIV, delineated by the dotted line). In Nav1.9, the paddle motifs are not identical and are therefore colored differently: purple, domain I paddle (DI); red, domain II paddle (DII); blue, domain III paddle (DIII); green, domain IV paddle (DIV). This color code is used in the other figures. In Kv2.1, the paddle motifs are identical and therefore have the same color (gray). (B and C) Transfer of the hNav1.9 paddle motifs into Kv2.1. Families of potassium currents (B) and tail current voltage–activation relationships (C) for each chimeric construct ($n = 16$; error bars represent SEM). Holding voltage was −90 mV, and the tail voltage was −50 mV (−80 mV for DII). Bars in B are 1 µA and 100 ms.

Toxins targeting hNav1.9 voltage sensors

Although canonical Nav channels are widely targeted by toxins from venomous organisms (Catterall et al., 2007; Swartz, 2007; Bosmans and Swartz, 2010), the pharmacological sensitivity of the hNav1.9 channel has not been explored because the channel cannot be heterologously expressed, and recording hNav1.9-mediated Na^+ currents in transfected Nav1.9 knockout mice DRG neurons is technically challenging (Ostman et al., 2008). One class of toxins found in scorpion and tarantula venom interacts with S3b–S4 paddle motifs within voltage sensors of voltage-activated ion channels to alter their gating properties (Rogers et al., 1996; Swartz and MacKinnon, 1997b; Cestèle et al., 1998; Li-Smerin and Swartz, 2000; Jiang et al., 2003a; Phillips et al., 2005; Alabi et al., 2007; Bosmans et al., 2008; Milescu et al., 2009), and in these instances, transferring the paddle motif between channels appropriately transfers toxin sensitivity (Alabi et al., 2007; Bosmans et al., 2008; Milescu et al., 2009). To investigate whether toxins from venomous organisms can interact with the paddle motifs in hNav1.9, we screened 18 toxins from tarantula, scorpion, and sea anemone venom against the four hNav1.9 paddle constructs and

observed six toxins that potently inhibit one or more of the chimeras (Figs. 3 and S5). The results for five representative toxins are shown in Fig. 3, which include those for the tarantula toxins PaurTx3 (Bosmans et al., 2006), ProTx-I, and ProTx-II (Middleton et al., 2002), and the scorpion toxins AaHII (Martin et al., 1987a,b) and TsVII (Céard et al., 1992). In this group, the β-scorpion toxin TsVII and the tarantula toxin ProTx-I stand out as having robust activity against constructs containing the paddle motifs from hNav1.9.

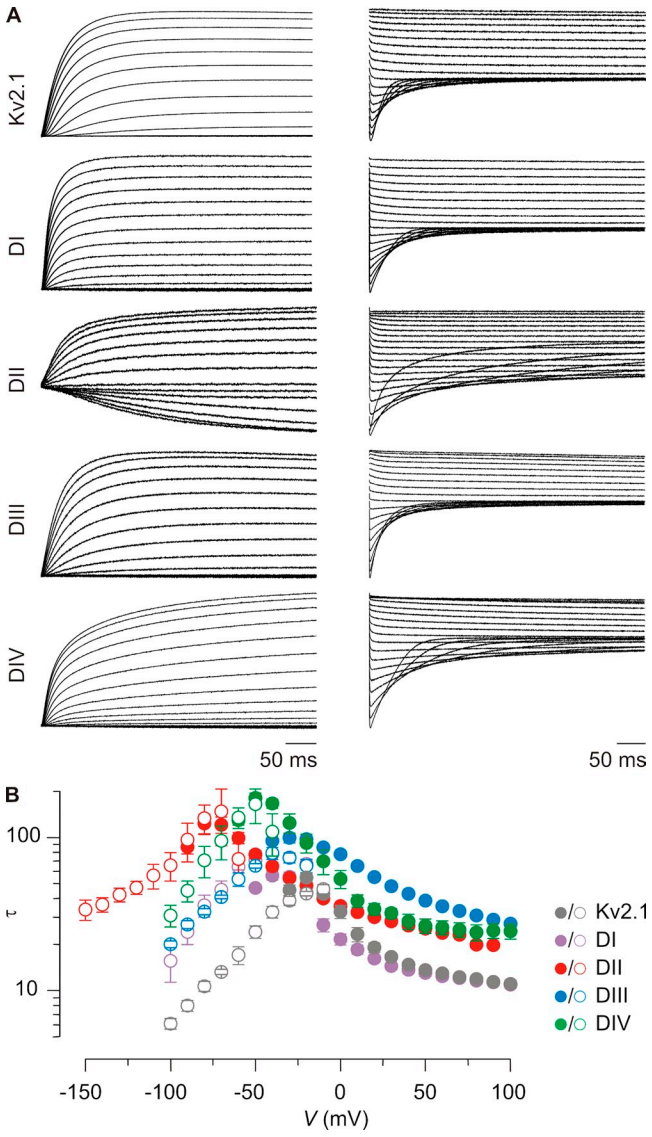

Figure 2. Kinetics of opening and closing for hNav1.9/Kv2.1 chimeric constructs. (A) Representative macroscopic currents showing channel activation (left) and channel deactivation (right) using the following voltage protocols: activation, 10-mV incrementing steps to voltages between −60 and +100 mV (−90 mV for DII) from a holding potential of −90 mV; deactivation, 10-mV incrementing steps to voltages between −10 and −100 mV (−150 mV for DII) from a test voltage of between +80 and +100 mV (holding potential is −90 mV). (B) Mean time constants (τ) from single-exponential fits to channel activation (filled circles) and deactivation (open circles) plotted as a function of the voltage at which the current was recorded. n = 4–8, and error bars represent SEM.

In the case of the β-scorpion toxin TsVII, transfer of the domain II, III, or IV paddle motifs from hNav1.9 renders Kv2.1 sensitive to the toxin, with the domain II chimera exhibiting the largest inhibition in the presence of 100 nM TsVII (Fig. 3). Because Kv2.1 is insensitive to TsVII, the interaction of the toxin with the domain II–IV paddle motifs is likely indicative of interactions in hNav1.9. In the case of ProTx-I, transfer of the domain III or IV paddle motifs of hNav1.9 dramatically increases the toxin sensitivity compared with wild-type Kv2.1. Although ProTx-I can interact weakly with Kv2.1 itself (Middleton et al., 2002; Bosmans et al., 2008), transfer of the domain I or II paddle motifs largely disrupts the effects of the toxin (Fig. 3), suggesting that the donor paddle motifs from hNav1.9 determine sensitivity to the toxin. Interpreting the results for the domain III chimera is not straightforward because this construct retains about half of the S3b helix from Kv2.1. However, the apparent affinity of ProTx-I is 10-fold higher for the domain III chimera (K_d = 173 ± 19 nM) compared with the Kv2.1 channel (K_d = 1,939 ± 153 nM) (Fig. S6 A), suggesting that the toxin can interact with the domain III paddle motif of hNav1.9. In addition, transfer of this paddle motif into Kv1.3 renders the channel more sensitive to ProTx-I (K_d = 116 ± 7nM) when compared with the Kv1.3 channel itself (K_d = 410 ± 58 nM) (Fig. S6 B). From these results, we conclude that ProTx-I does interact with the paddle motif from domain III of hNav1.9. The results with the domain IV chimera are more straightforward, and strongly suggest that ProTx-I also interacts with the paddle motif of this voltage sensor in hNav1.9. AaHII, as well as PaurTx3 and ProTx-II, provide clear examples of toxins that do not target the Kv2.1 channel or any of the chimeras containing paddle motifs from hNav1.9 (Fig. 3).

It is interesting that the profile of toxin–paddle interactions observed here for hNav1.9 is different from that of the rNav1.2a isoform (Bosmans et al., 2008) (Fig. S7). A striking example is the inability of ProTx-II to interact with any of the hNav1.9 paddles, whereas three out of four paddle motifs in rNav1.2a are targeted. Conversely, PaurTx3 does not influence any of the hNav1.9 paddle constructs, but it robustly inhibits the rNav1.2a domain II paddle construct. AaHII interacts only weakly with the paddle motifs from domains II and IV from hNav1.9, whereas the toxin selectively and strongly targets the domain IV paddle motif within rNav1.2a. ProTx-I interacts with the paddle motif from domains III and IV from hNav1.9, yet the toxin targets domains II and IV in rNav1.2a. TsVII is unique among the five toxins in that it has a similar pharmacological profile for paddle motifs from hNav1.9 and rNav1.2a. These distinct profiles

for hNav1.9 and rNav1.2a likely reflect the fact that the sequences of the S3b–S4 regions in these two channels are strikingly dissimilar. Indeed, the paddle motifs for the canonical Nav1.1–Nav1.7 channels are highly similar when comparing the same domains, whereas the paddle motifs in both rNav1.8 and hNav1.9 stand out as unique (Fig. S2).

Functional properties of rNav1.9 voltage sensors

Our ultimate objective was to test whether the toxin–channel interactions identified using our chimeras actually occur with Nav1.9 channels in rat DRG neurons. Recognizing that the human and rat orthologues of Nav1.9 are not identical, we first constructed and studied the analogous Kv2.1 chimeras containing the paddle motifs from rNav1.9. Although the amino acid sequence of the rat and human orthologue differ significantly (percentage of conserved residues for the paddle motifs in domains I, II, III, and IV is 64, 64, 86, and 88, respectively), we were able to generate a set of functional Kv2.1 channels containing S3b–S4 paddle regions from the four voltage sensors in rNav1.9 (Figs. 4 and S2, and Table S1). The G-V relations observed for these rNav1.9 chimeras were remarkably similar, and like hNav1.9/Kv2.1 chimeras, the constructs containing the paddle motifs from domains II, III, and IV exhibited relatively slow kinetics (Fig. 4).

Next, we tested the sensitivity of the rNav1.9 constructs to TsVII and ProTx-I, the two toxins that stood out as having robust activity against hNav1.9 chimeras. Similar to what was observed with the human constructs, Kv2.1 channels containing the domain II paddle motif from rNav1.9 are sensitive to TsVII. In contrast to the human orthologue, transferring the paddle motifs from the remaining three rNav1.9 voltage sensors into Kv2.1 generates little or no sensitivity to the toxin (Figs. 3 and 4). In the case of ProTx-I, inserting the domain I, III, or IV

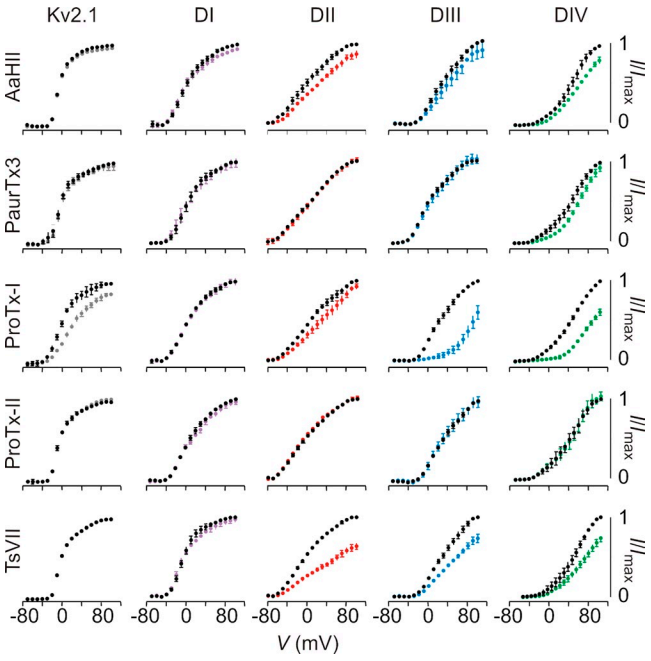

Figure 3. Sensitivity of hNav1.9/Kv2.1 constructs to extracellular toxins. Effects of toxins on Kv2.1 and chimeric constructs where paddle motifs were transferred from hNav1.9 into Kv2.1. Normalized tail current voltage–activation relationships are shown where tail current amplitude is plotted against test voltage before (black) and in the presence of toxin (other colors). Data are grouped per toxin (horizontally) and per chimera or wild-type Kv2.1 (vertically). Concentrations used are 100 nM PaurTx3, ProTx-I, ProTx-II, and TsVII, and 1 µM AaHII. The holding voltage was −90 mV, the test pulse duration was 300 ms, and the tail voltage was −50 mV (−80 mV for DII). n = 3–5, and error bars represent SEM.

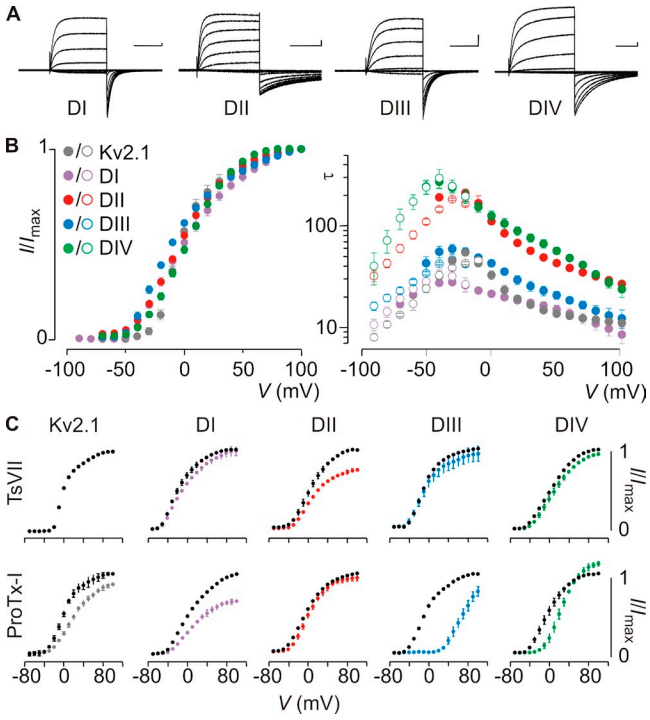

Figure 4. Sensitivity of rNav1.9/Kv2.1 constructs to extracellular toxins. (A) Families of potassium currents, (B, left) tail current voltage–activation relationships, and (B, right) kinetics of opening and closing for Kv2.1 channels containing paddle motifs from the four domains of rNav1.9 for each chimeric construct (n = 8, and error bars represent SEM). Holding voltage was −90 mV, and the tail voltage was −60 mV. Bars in A are 0.5 µA and 100 ms (200 ms for DII and DIV). Mean time constants (τ) from single-exponential fits to channel activation (filled circles) and deactivation (open circles) are plotted as a function of the voltage at which the current was recorded. (C) Effects of TsVII and ProTx-I on Kv2.1 and chimeric constructs where paddle motifs were transferred from rNav1.9 into Kv2.1. Normalized tail current voltage–activation relationships are shown where tail current amplitude is plotted against test voltage before (black) and in the presence of toxin (other colors). Concentration used is 100 nM. Apparent K_d of TsVII for the DII construct is 202 ± 6 nM. Apparent K_d of ProTx-I for DI, DIII, and DIV is 412 ± 8 nM, 77 ± 21 nM, and 133 ± 36 nM, respectively (calculated K_d assuming four independent toxin-binding sites per channel). The holding voltage was −90 mV, the test pulse duration was 300 ms, and the tail voltage was −60 mV. n = 3–5, and error bars represent SEM.

paddle motifs from rNav1.9 dramatically increases the toxin sensitivity of Kv2.1, whereas transferring the domain II paddle motif into Kv2.1 largely disrupts the effects of the toxin (Fig. 4). This pattern is similar to what we observe with hNav1.9, except that (a) ProTx-I targets an additional paddle motif in domain I of rNav1.9; and (b) at negative voltages, ProTx-I inhibits the opening of Kv2.1 containing the rNav1.9 domain IV paddle motif, whereas channel opening is enhanced at more depolarized voltages. This interesting feature is also observed when the tarantula toxin ω-grammotoxin-SIA is applied to P- and N-type calcium channels (McDonough et al., 1997), and suggests an enhanced probability of channel opening or an increase in single-channel conductance at positive voltages.

Collectively, these data show that both hNav1.9 and rNav1.9 channels contain S3b–S4 paddle motifs that can be targeted by animal toxins. Two toxins in particular, TsVII and ProTx-I, appear to be especially promising tools to investigate Nav1.9-mediated currents in DRG neurons.

Comparing Nav1.8 and Nav1.9 voltage sensor pharmacology

A key obstacle in identifying and studying Nav1.9-mediated Na^+ currents in rat DRG neurons is the presence of rNav1.8 channels, which open and inactivate in overlapping voltage ranges (Maruyama et al., 2004) and like Nav1.9, are resistant to high concentrations of TTX (i.e., TTX-r). To evaluate the utility of ProTx-I and TsVII as tools to study rNav1.9 channels in native neurons, we first investigated the interaction of these toxins with rNav1.8. Although the β-scorpion toxin TsVII produces robust inhibition of the domain II rNav1.9 paddle chimera at 100 nM, this concentration of the toxin is without effect on rNav1.8 (Fig. 5, A and B), and even at 1 µM produces only modest inhibition of the channel (Fig. 5, C and D). When using protocols containing short depolarizing prepulses (Cestèle et al., 1998), TsVII does not shift activation of rNav1.8 to negative voltages, although the modest inhibitory effect observed at high concentrations is somewhat enhanced (Fig. 5, C and D). These results suggest that TsVII would be useful in distinguishing between rNav1.8 and rNav1.9 in neurons, particularly when tested at low concentrations.

In contrast to TsVII, ProTx-I does influence rNav1.8 and was actually discovered in a search for inhibitors of that Nav channel isoform (Middleton et al., 2002). To investigate the utility of ProTx-I in characterizing Nav1.9 channels in rat DRG neurons, we examined the concentration dependence for inhibition of rNav1.8 and determined which paddle motifs are targeted by the toxin. At 100 nM, ProTx-I produces robust inhibition of rNav1.8 and shifts activation to positive voltages (Fig. 6, A–C). When the concentration dependence for inhibition at negative voltages was fitted with a Hill equation, an IC_{50} of ∼11 nM and a slope of 1.3 were obtained (Fig. 6 D), suggesting that the toxin interacts with multiple sites. Similar to what was observed for rNav1.9, three paddle motifs from rNav1.8 (I, III, and IV) are targeted by the toxin (Figs. 6 E and S8).

Collectively, these results suggest that TsVII will preferentially interact with Nav1.9 channels in rat DRG neurons, and that ProTx-I will affect both rNav1.8 and rNav1.9. However, the effects of ProTx-I on these two channels might differ because the states stabilized by voltage sensor toxins are not always recapitulated in paddle chimeras, and the role of individual voltage sensors in the gating of these two Nav channel isoforms has not yet been explored (see Discussion).

Pharmacological sensitivity of Nav1.8 and Nav1.9 currents in rat DRG neurons

Having identified two toxins that target rNav1.9, we investigated their actions on native Na^+ currents carried by Nav1.9 in rat DRG neurons. Previous work has shown that Nav1.9 channels carry a component of TTX-r Na^+ current in small DRG neurons that activates at unusually negative voltages and inactivates very slowly (Cummins et al., 1999; Maruyama et al., 2004; Priest et al., 2005; Binshtok et al., 2007; Coste et al., 2007; Maingret et al., 2008; Ostman et al., 2008; Leo et al., 2010). With TTX-sensitive currents blocked, rNav1.9-mediated current

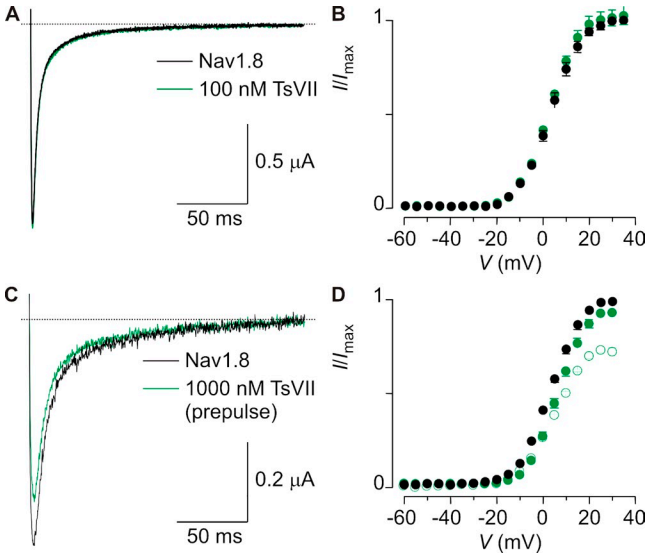

Figure 5. Effect of TsVII on rNav1.8. (A) rNav1.8 currents at +15 mV are not affected by 100 nM TsVII (holding voltage was −90 mV). (B) G-V relationship of rNav1.8 before (black) and after (green) the application of 100 nM TsVII. $n = 3$, and error bars represent SEM. (C) rNav1.8 currents at +15 mV are only slightly inhibited when 1 µM TsVII is applied in combination with a preceding 5-ms depolarizing pulse to +30 mV (holding voltage was −90 mV) (Cestèle et al., 1998). (D) Deduced G-V relationship of rNav1.8 before (black) and after (green) the application of 100 nM TsVII. Open circles indicate the use of a depolarizing prepulse. $n = 3$, and error bars represent SEM.

can be distinguished from rNav1.8-mediated current by a requirement for strongly negative holding potentials and by its slow activation and inactivation kinetics at voltages near −60 mV; in contrast, rNav1.8-mediated current retains nearly full availability at holding potentials as positive as −50 mV and is first activated by steps near −20 mV (Blair and Bean, 2002). Fig. 7 shows recordings from a small rat DRG neuron, using a pulse protocol expected to activate predominantly rNav1.9-mediated currents. With TTX in the recording solution, steps to voltages between −55 and −35 mV activate very little current when the holding potential was set to −80 mV. However, when the holding potential is changed to −120 mV, there is a dramatic enhancement of the current activated between −55 and −35 mV. This current inactivates very slowly, with decay by 50 ± 14% (mean ± SD; n = 14) over 2 s at −50 mV. This slow inactivation is very similar to the properties of Nav1.9 previously reported (Cummins et al., 1999; Maruyama et al., 2004; Baker, 2005; Priest et al., 2005; Coste et al., 2007; Maingret et al., 2008; Ostman et al., 2008; Copel et al., 2009).

We began exploring the pharmacological sensitivity of native rNav1.9 channels by investigating the effects of the β-scorpion toxin TsVII. Consistent with its ability to interact with voltage sensor motifs from Nav1.9, TsVII has a large effect on rNav1.9-mediated currents with

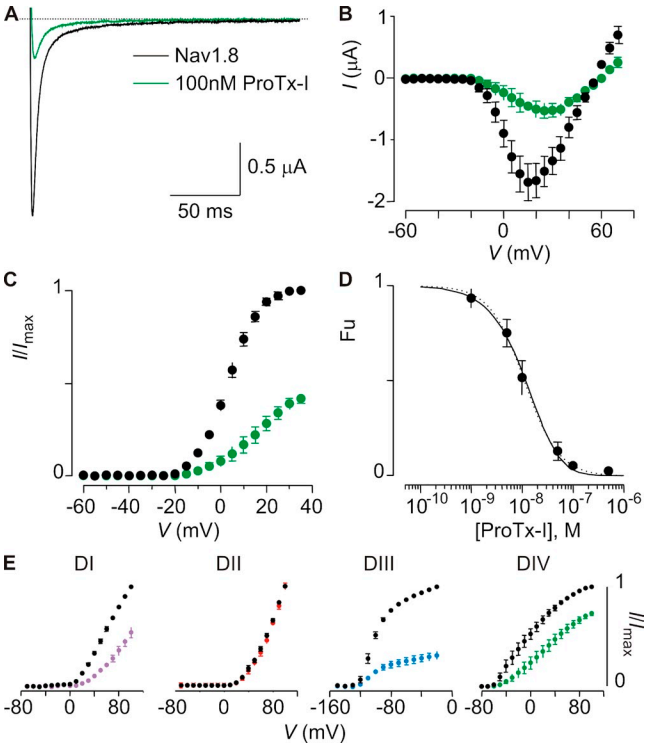

Figure 6. Inhibition of rNav1.8 by ProTx-I. (A) Inhibition of rNav1.8 currents by 100 nM ProTx-I at +15 mV (holding voltage was −90 mV). (B and C) Current–voltage relationship (B) and deduced G-V relationship (C) of rNav1.8 before (black) and after (green) the application of 100 nM ProTx-I. n = 3–5, and error bars represent SEM. (D) Concentration dependence for ProTx-I inhibition of rNav1.8 plotted as fraction unbound (Fu) measured at negative voltages. Dotted line is a fit of the Hill equation to the data (IC_{50} = 10.9 ± 0.5 nM; slope = 1.3 ± 0.1). Solid line is a fit with a three-binding site model (K_d = 45.1 ± 2.7 nM). See Materials and methods for more information. (E) Effect of 100 nM ProTx-I on Kv2.1 channels containing paddle motifs from rNav1.8. Normalized tail current voltage–activation relationships are shown before and after the application of the toxin. n = 4, and error bars represent SEM.

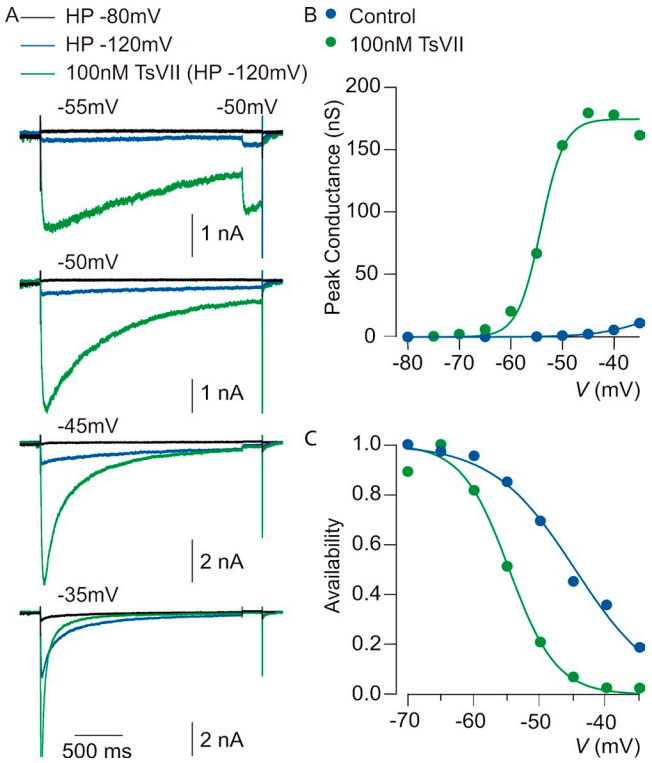

Figure 7. Effect of TsVII on native Nav1.9 currents in rat DRG neurons. (A) Enhancement by 100 nM TsVII of TTX-r current evoked by steps to voltages between −55 and −35 mV. Control currents were recorded with a steady holding potential of either −80 mV (black traces) or −120 mV (blue traces), established for >5 min to remove inactivation from rNav1.9 channels. In both cases, the test pulse was preceded by a 400-ms step to −140 mV. 100 nM TsVII (green traces) was applied at the holding potential of −120 mV. (B) Peak conductance versus test voltage before and after 100 nM TsVII (different cell than A). Closed symbols, peak conductance calculated from peak current using a reversal potential of +50 mV; smooth curves, best fits to a Boltzmann function according to $G = G_{max}/(1 + e^{-(V - V_{1/2})/k})$, where G_{max} is the maximal conductance, $V_{1/2}$ is the half-activation voltage, and k is the slope factor. Control: G_{max} = 25 nS, $V_{1/2}$ = −34 mV, and k = 4.9 mV. 100 nM TsVII: G_{max} = 174 nS, $V_{1/2}$ = −54 mV, and k = 2.3 mV. (C) Voltage dependence of inactivation determined using a test pulse to −50 mV from a variety of holding potentials established for 2 s. Smooth curves are best fits to a Boltzmann function according to: $I/I_{max} = (1 + e^{(V - V_{1/2})/k})^{-1}$, where I/I_{max} is the normalized peak conductance, $V_{1/2}$ is the midpoint of inactivation, and k is the slope factor. Control: $V_{1/2}$ = −45 mV and k = 6.2 mV. 100 nM TsVII: $V_{1/2}$ = −55 mV and k = 3.6 mV. All solutions contained 300 nM TTX to block TTX-s Nav channels.

characteristics suggesting interaction with the voltage-sensing machinery of the channel. At 100 nM, TsVII produces a dramatic enhancement of current evoked by steps to voltages between −55 and −35 mV (Fig. 7 A). The most frequently observed effect of β-scorpion toxins on Nav channels is to shift opening to more negative voltages by stabilizing the voltage sensors in an activated conformation (Cestèle et al., 1998; Campos et al., 2007). Although we can only study rNav1.9 currents in isolation over a relatively narrow voltage range (because rNav1.8 current begins to activate positive to −30 mV), plotting the voltage dependence of peak conductance as a function of voltage suggests that TsVII shifts the voltage dependence of activation to more hyperpolarized voltages (Fig. 7 B and Table I). In most cells, there is insufficient saturation of the conductance versus voltage curve to accurately fit Boltzmann functions, but a shift of voltage dependence by TsVII is clearly manifested by a much greater enhancement of currents at −55 mV (increase by an average factor of 46 ± 79) compared with −35 mV (increase by an average factor of 5.0 ± 4.7; mean ± SD; $n = 7$; P = 0.016; Wilcoxon test). We also examined the voltage dependence of inactivation of rNav1.9 channels by delivering 2-s prepulses and then assaying availability with a test pulse to −50 mV. The midpoint of inactivation is shifted in the hyperpolarizing direction by TsVII (Fig. 7 C and Table I). On average, the midpoint of inactivation changes from −46.9 ± 4.9 mV in control to −53.4 ± 3.9 mV when 100 nM TsVII is applied (mean ± SD; $n = 7$; P = 0.031; Wilcoxon test).

Next, we examined the actions of ProTx-I, the tarantula toxin that we found to interact primarily with rNav1.9 paddle motifs from domains III and IV. Similar to TsVII, ProTx-I produces a dramatic facilitation of rNav1.9 currents elicited by steps between −55 and −35 mV (Fig. 8 A). Also similar to what is observed with TsVII, ProTx-I appears to shift both activation and inactivation of rNav1.9 to more negative voltages (Fig. 8, B and C, and Table I). At 100 nM, ProTx-I enhances currents at −55 mV by a greater factor (4.6 ± 1.8) than at −35 mV (2.5 ± 2.0; mean ± SD; $n = 5$; P = 0.063; Wilcoxon test), consistent with a mechanism involving altered voltage dependence. The midpoint of inactivation also changes from −48.7 ± 4.1 mV in control to −50.1 ± 3.9 mV (mean ± SD; $n = 5$; P = 0.43; Wilcoxon test) (Table I).

TABLE I

Gating properties of Nav1.9-mediated currents in rat DRG neurons without and in the presence of 100 nM ProTx-I and TsVII

No toxin	100 nM ProTx-I	No toxin	100 nM TsVII
Activation ($V_{1/2}$)		Activation ($V_{1/2}$)	
−42.1 ± 2.5 mV	−44.6 ± 2.2 mV	−42.1 ± 0.9 mV	−46.8 ± 4.0 mV
Inactivation ($V_{1/2}$)		Inactivation ($V_{1/2}$)	
−48.7 ± 4.1 mV	−50.1 ± 3.9 mV	−46.9 ± 4.9 mV	−53.4 ± 3.9 mV

The similar effects of ProTx-I and TsVII on native rNav1.9 channels is especially interesting because the experiments with heterologously expressed rNav1.8 channels shows that ProTx-I inhibits the channels, whereas TsVII has little or no effect. We therefore examined the effects of the two toxins on rNav1.8 channels in DRG neurons (Fig. 9). Very similar to the results with) heterologously expressed channels, native rNav1.8 currents (elicited by a step from −50 to 0 mV) are affected only slightly by TsVII, whereas ProTx-I produces substantial inhibition. On average, the peak rNav1.8 current after 100 nM TsVII is reduced by 15 ± 10% (mean ± SD; $n = 8$), whereas the peak current after 100 nM ProTx-I is reduced by 56 ± 16% (mean ± SD; $n = 11$), consistent with previous results (Priest et al., 2007).

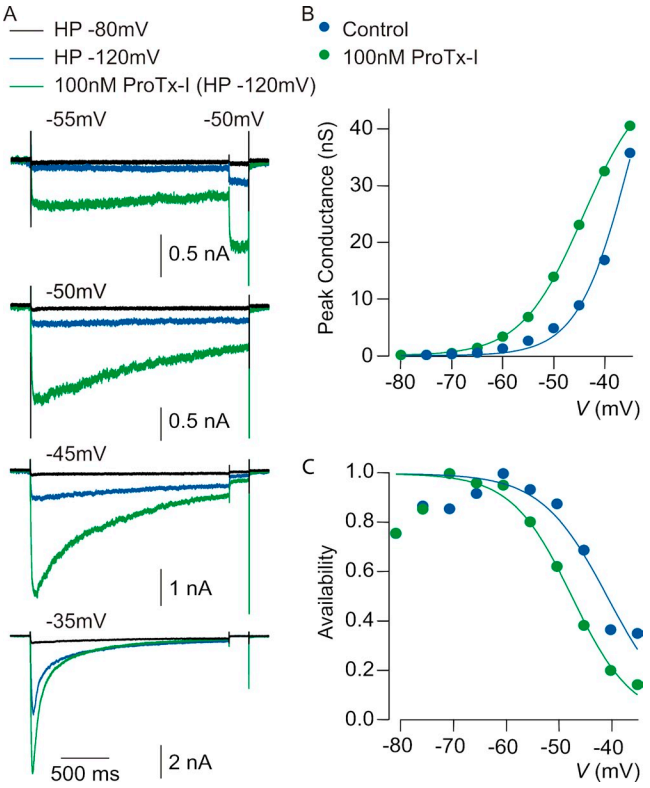

Figure 8. Effect of ProTx-I on native Nav1.9 currents in rat DRG neurons. (A) Enhancement by 100 nM ProTx-I of rNav1.9-mediated current evoked by same protocol as in Fig. 7 A. (B) Peak conductance versus test voltage before and after 100 nM ProTx-I (different cell than A). Closed symbols, peak conductance calculated from peak current using a reversal potential of +50 mV; smooth curves, best fits to a Boltzmann function, as in Fig. 7 B. Control: G_{max} = 70 nS, $V_{1/2}$ = −35 mV, and k = 5.0 mV. 100nm ProTx-I: G_{max} = 49 nS, $V_{1/2}$ = −44 mV, and k = 6.0 mV. (C) Voltage dependence of inactivation determined using a test pulse to −50 mV from a variety of holding potentials established for 2 s as in Fig. 7 C. Smooth curves are best fits to Boltzmann functions. Control: $V_{1/2}$ = −41 mV and k = 6.2 mV. 100 nM ProTx-I: $V_{1/2}$ = −47 mV and k = 5.6 mV. All solutions contained 300 nM TTX to block TTX-s Nav channels.

Collectively, the results with TsVII and ProTx-I suggest that these toxins can interact with rNav1.9 in its native environment. The actions of ProTx-I are particularly interesting because the toxin has opposite effects on rNav1.8 and rNav1.9, the two TTX-r channels expressed in DRG neurons, enhancing rNav1.9 current but inhibiting rNav1.8 current.

DISCUSSION

The goal of this study was to explore the functional and pharmacological properties of Nav1.9, a non-canonical Nav channel that in native neurons displays unusually slow activation and inactivation kinetics (Cummins et al., 1999; Blum et al., 2002; Maruyama et al., 2004; Priest et al., 2005; Coste et al., 2007; Ostman et al., 2008). By taking advantage of the portable nature of S3b–S4 paddle motifs within voltage-sensing domains (Alabi et al., 2007; Bosmans et al., 2008; Milescu et al., 2009), we show that such motifs exist in each of the four voltage-sensing domains of human and rat Nav1.9, and that they can be transplanted into Kv channels and studied in isolation (Fig. 1). Our results reveal that each of the Nav1.9 paddle motifs can sense changes in membrane voltage and drive voltage sensor activation within Kv channels, similar to what has been found for canonical Nav channels (Bosmans et al., 2008). Because the pharmacological sensitivities of Nav1.9 remain unexplored, we exploited these paddle constructs to search for toxins that might interact with Nav1.9 channels. We found that the Nav1.9 paddle motifs from all four domains can interact with toxins from scorpion or tarantula venom (Figs. 3 and 4), providing a clear parallel between Nav1.9 and canonical Nav channels.

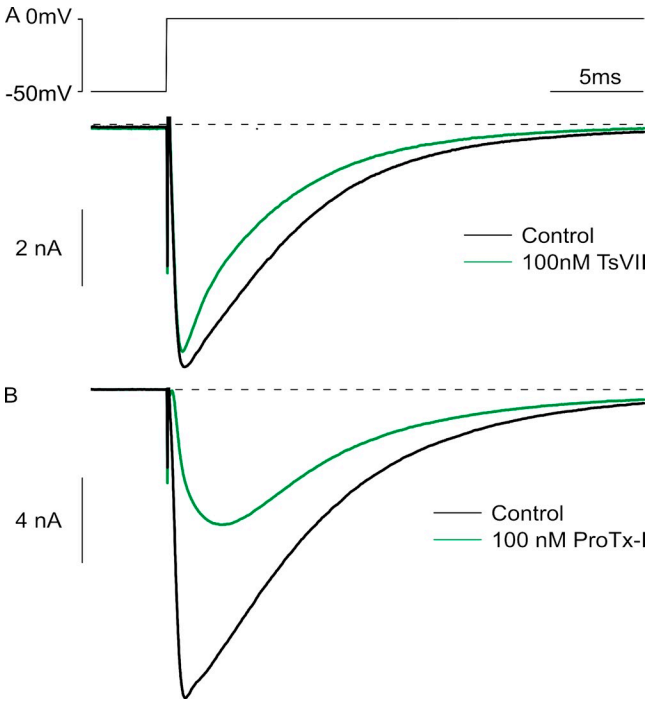

Figure 9. Effect of TsVII and ProTx-I on native Nav1.8 currents in rat DRG neurons. (A) Effect of 100 nM TsVII on rNav1.8-mediated current, evoked by a step from a holding potential of −50 mV in the presence of 300 nM TTX. (B) Effect of 100 nM ProTx-I on native rNav1.8-mediated current.

The two most interesting toxins emerging from our screens are the scorpion toxin TsVII and the tarantula toxin ProTx-I, both of which interact with Nav1.9 paddle motifs (Figs. 3 and 4) and potently facilitate the low-threshold, slowly activating and inactivating sodium current in rat DRG neurons (Figs. 7 and 8) that has been ascribed to Nav1.9 (Cummins et al., 1999; Maruyama et al., 2004; Priest et al., 2005; Coste et al., 2007; Ostman et al., 2008). In addition to targeting rNav1.9 in DRG neurons, TsVII and ProTx-I have very different actions on rNav1.8, the other TTX-r Nav channel present in these sensory neurons. At a concentration of 100 nM, TsVII produces a dramatic facilitation of rNav1.9 currents (Fig. 7 B) while only modestly inhibiting rNav1.8, either when heterologously expressed (Fig. 5) or in native neurons (Fig. 9), showing that the scorpion toxin can discriminate between these two TTX-r Nav channels. At the same concentration, ProTx-I causes both a pronounced potentiation of rNav1.9 currents (Fig. 8) and a robust inhibition of rNav1.8 (Figs. 6 and 9). Collectively, these findings provide strong evidence that TsVII and ProTx-I strongly interact with native rNav1.9 channels. Moreover, our collective results with a wide range of toxins demonstrate that Nav1.9 has different pharmacological sensitivities than other Nav channel isoforms (Figs. 3, 4, S5, and S7).

Although previous studies have shown that sensitivity to tarantula and scorpion toxins can be transferred along with paddle motifs (Alabi et al., 2007; Bosmans et al., 2008; Milescu et al., 2009), the resulting effects on channel gating are sometimes paradoxical and difficult to predict. One example has been observed for α-scorpion toxins, a class of toxins that interacts with the voltage sensor in domain IV and interferes with Nav channel fast inactivation (Rogers et al., 1996; Leipold et al., 2004). Sensitivity to α-scorpion toxins can be transferred to Kv channels along with domain IV paddle motifs, but in the context of these chimeras, the toxin inhibits the channel by stabilizing a closed state (Bosmans et al., 2008). The difference in activity of the toxin could be explained if the toxin stabilized related resting (or intermediate) states of the voltage sensors in both Nav and Kv channels, but full voltage sensor activation is required for inactivation in Nav channels or for opening in Kv channels (Campos et al., 2008). In this scenario, the states that are stabilized in the two channels are related, but the voltage sensors couple to distinct gating transitions. Another example has been reported for β-scorpion toxins, a family of toxins that facilitate Nav channel activity by shifting opening to more negative voltages by interacting with the voltage sensor in domain II

and stabilizing it in an activated state (Marcotte et al., 1997; Cestèle et al., 1998, 2006; Campos et al., 2007; Bosmans et al., 2008). Previous experiments show that the sensitivity to the β-scorpion toxin TsVII can be transferred to Kv channels along with the domain II paddle motif of rNav1.2a and rNav1.4, but in the context of these chimeras, the toxin inhibits by stabilizing a closed state (Bosmans et al., 2008). Although the mechanism for stabilizing distinct states in Kv and Nav channels is unknown, this discrepancy suggests that other regions of the channel or the membrane environment play important roles in determining which states are stabilized. The present results with TsVII and rNav1.9 are reminiscent of what was observed with rNav1.2a because the toxin inhibits Kv channel chimeras while facilitating the opening of Nav1.9 channels in rat DRG neurons (Figs. 3, 4, and 7). ProTx-I also facilitates the opening of rNav1.9 while inhibiting Kv channels containing paddle motifs from either domain III or IV of the Nav channel, similar to what is observed with TsVII (Figs. 3, 4, and 8). Interestingly, the present results with rNav1.9 suggest that ProTx-I does not interact with the paddle motif in domain II, the domain most commonly targeted by β-scorpion toxins in other Nav channel isoforms. If the roles of the four voltage sensors in rNav1.9 gating are similar to canonical Nav channels, ProTx-I may work by stabilizing the voltage sensors from domain III and/or domain IV in a fully activated state.

Accumulating evidence suggests that Nav1.9 plays a particularly important functional role in the excitability of primary sensory neurons under conditions where the neurons become hyperexcitable on exposure to inflammatory mediators (Rush and Waxman, 2004; Binshtok et al., 2007; Maingret et al., 2008; Ostman et al., 2008; Copel et al., 2009). In the absence of such mediators, current carried by Nav1.9 channels appears to be negligible unless physiologically irrelevant holding potentials are established (Figs. 7 A and 8 A). However, there is a dramatic enhancement of Nav1.9-mediated current by a variety of inflammatory mediators (Rush and Waxman, 2004; Binshtok et al., 2007; Copel et al., 2009) or if G protein pathways are activated by GTP-γ-S (Baker et al., 2003; Baker, 2005; Ostman et al., 2008), in which case substantial Nav1.9 currents appear at the resting potential, resulting in cell depolarization and hyperexcitability. A particularly dramatic enhancement of Nav1.9-mediated current can be produced by simultaneous application of multiple inflammatory mediators in an "inflammatory soup" (Maingret et al., 2008), suggestive of a large reserve of Nav1.9 channels that can be recruited by modulatory pathways. Our results with TsVII and ProTx-I also suggest a large pool of rNav1.9 channels that are present but not activated under normal conditions: 100 nM TsVII enhances the current evoked from a holding potential of −120 mV by an average of 35-fold (for a step to −50 mV), and the combined effect of changing the holding potential from −80 to −120 mV and applying 100 nM TsVII results in an average enhancement of current at −50 mV by 89-fold.

Although the actions of TsVII and ProTx-I on human and rat Nav1.9 demonstrate that this unusual Nav channel has structural features and functional properties that are similar to canonical Nav channels, these toxins themselves are not suitable for in vivo experiments geared toward exploring the role of Nav1.9 in pain transmission and other physiological responses because both toxins interact with other voltage-activated ion channels. TsVII also facilitates the opening of rNav1.2a (Bosmans et al., 2008) and rNav1.4 channels (Campos et al., 2007), whereas ProTx-I inhibits several other Nav channel isoforms and Cav3.1 channels (Middleton et al., 2002), making it difficult to trace any actions of the toxins back to Nav1.9. However, the effects of the toxins clearly show that Nav1.9 paddle motifs constitute an attractive pharmacological target and also demonstrate the possibility of discriminating between Nav1.8 and Nav1.9, with agents targeting the gating machinery of the channels. More broadly, the results show that making chimeras using paddle motifs grafted onto a Kv channel backbone can be used as an effective strategy for identifying pharmacological agents capable of interacting with channels whose full heterologous expression is difficult or impossible. This chimera strategy should be of wide utility for setting up novel screening programs for a variety of difficult-to-express voltage-activated channels. Given the important role of Nav1.9 in inflammatory and diabetic neuropathy pain (Dib-Hajj et al., 2010), such an approach targeted at Nav1.9 channels seems promising as a new strategy for developing novel pain treatments.

We thank R. Blum and J.N. Wood for the hNav1.9 and rNav1.8 clones, C. Deutsch for Kv1.3, L.L. Isom for β1, M.M. Smith for ProTx-II, K.M. Blumenthal for Ap-B, and J.I. Kim for GxTx-1E. We also thank Miguel Holmgren, Mark Mayer, Joe Mindell, Shai Silberberg, and members of the Swartz laboratory for helpful discussions.

This work was supported by the Intramural Research Program of the National Institute of Neurological Disorders and Stroke, National Institutes of Health.

Stephen C. Cannon served as guest editor.

Submitted: 10 February 2011
Accepted: 24 May 2011

REFERENCES

Aggarwal, S.K., and R. MacKinnon. 1996. Contribution of the S4 segment to gating charge in the Shaker K+ channel. *Neuron.* 16:1169–1177. doi:10.1016/S0896-6273(00)80143-9

Akopian, A.N., L. Sivilotti, and J.N. Wood. 1996. A tetrodotoxin-resistant voltage-gated sodium channel expressed by sensory neurons. *Nature.* 379:257–262. doi:10.1038/379257a0

Akopian, A.N., V. Souslova, S. England, K. Okuse, N. Ogata, J. Ure, A. Smith, B.J. Kerr, S.B. McMahon, S. Boyce, et al. 1999. The tetrodotoxin-resistant sodium channel SNS has a specialized function in pain pathways. *Nat. Neurosci.* 2:541–548. doi:10.1038/9195

Alabi, A.A., M.I. Bahamonde, H.J. Jung, J.I. Kim, and K.J. Swartz. 2007. Portability of paddle motif function and pharmacology in voltage sensors. *Nature.* 450:370–375. doi:10.1038/nature06266

Amaya, F., H. Wang, M. Costigan, A.J. Allchorne, J.P. Hatcher, J. Egerton, T. Stean, V. Morisset, D. Grose, M.J. Gunthorpe, et al. 2006. The voltage-gated sodium channel Na(v)1.9 is an effector of peripheral inflammatory pain hypersensitivity. *J. Neurosci.* 26:12852–12860. doi:10.1523/JNEUROSCI.4015-06.2006

Baker, M.D. 2005. Protein kinase C mediates up-regulation of tetrodotoxin-resistant, persistent Na+ current in rat and mouse sensory neurones. *J. Physiol.* 567:851–867. doi:10.1113/jphysiol.2005.089771

Baker, M.D., and J.N. Wood. 2001. Involvement of Na+ channels in pain pathways. *Trends Pharmacol. Sci.* 22:27–31. doi:10.1016/S0165-6147(00)01585-6

Baker, M.D., S.Y. Chandra, Y. Ding, S.G. Waxman, and J.N. Wood. 2003. GTP-induced tetrodotoxin-resistant Na+ current regulates excitability in mouse and rat small diameter sensory neurones. *J. Physiol.* 548:373–382. doi:10.1113/jphysiol.2003.039131

Bezanilla, F., E. Perozo, and E. Stefani. 1994. Gating of Shaker K+ channels: II. The components of gating currents and a model of channel activation. *Biophys. J.* 66:1011–1021. doi:10.1016/S0006-3495(94)80882-3

Binshtok, A.M., B.P. Bean, and C.J. Woolf. 2007. Inhibition of nociceptors by TRPV1-mediated entry of impermeant sodium channel blockers. *Nature.* 449:607–610. doi:10.1038/nature06191

Blair, N.T., and B.P. Bean. 2002. Roles of tetrodotoxin (TTX)-sensitive Na+ current, TTX-resistant Na+ current, and Ca2+ current in the action potentials of nociceptive sensory neurons. *J. Neurosci.* 22:10277–10290.

Blum, R., K.W. Kafitz, and A. Konnerth. 2002. Neurotrophin-evoked depolarization requires the sodium channel Na(V)1.9. *Nature.* 419:687–693. doi:10.1038/nature01085

Bosmans, F., and K.J. Swartz. 2010. Targeting voltage sensors in sodium channels with spider toxins. *Trends Pharmacol. Sci.* 31:175–182. doi:10.1016/j.tips.2009.12.007

Bosmans, F., L. Rash, S. Zhu, S. Diochot, M. Lazdunski, P. Escoubas, and J. Tytgat. 2006. Four novel tarantula toxins as selective modulators of voltage-gated sodium channel subtypes. *Mol. Pharmacol.* 69:419–429. doi:10.1124/mol.105.015941

Bosmans, F., M.F. Martin-Eauclaire, and K.J. Swartz. 2008. Deconstructing voltage sensor function and pharmacology in sodium channels. *Nature.* 456:202–208. doi:10.1038/nature07473

Campos, F.V., B. Chanda, P.S. Beirão, and F. Bezanilla. 2007. β-Scorpion toxin modifies gating transitions in all four voltage sensors of the sodium channel. *J. Gen. Physiol.* 130:257–268. doi:10.1085/jgp.200609719

Campos, F.V., B. Chanda, P.S. Beirão, and F. Bezanilla. 2008. α-Scorpion toxin impairs a conformational change that leads to fast inactivation of muscle sodium channels. *J. Gen. Physiol.* 132:251–263. doi:10.1085/jgp.200809995

Catterall, W.A. 2000. From ionic currents to molecular mechanisms: the structure and function of voltage-gated sodium channels. *Neuron.* 26:13–25. doi:10.1016/S0896-6273(00)81133-2

Catterall, W.A., S. Cestèle, V. Yarov-Yarovoy, F.H. Yu, K. Konoki, and T. Scheuer. 2007. Voltage-gated ion channels and gating modifier toxins. *Toxicon.* 49:124–141. doi:10.1016/j.toxicon.2006.09.022

Céard, B., M.E. De Lima, P.E. Bougis, and M.F. Martin-Eauclaire. 1992. Purification of the main beta-toxin from Tityus serrulatus scorpion venom using high-performance liquid chromatography. *Toxicon.* 30:105–110. doi:10.1016/0041-0101(92)90506-Z

Cestèle, S., Y. Qu, J.C. Rogers, H. Rochat, T. Scheuer, and W.A. Catterall. 1998. Voltage sensor-trapping: enhanced activation of sodium channels by beta-scorpion toxin bound to the S3-S4 loop in domain II. *Neuron.* 21:919–931. doi:10.1016/S0896-6273(00)80606-6

Cestèle, S., M. Stankiewicz, P. Mansuelle, M. De Waard, B. Dargent, N. Gilles, M. Pelhate, H. Rochat, M.F. Martin-Eauclaire, and D. Gordon. 1999. Scorpion alpha-like toxins, toxic to both mammals and insects, differentially interact with receptor site 3 on voltage-gated sodium channels in mammals and insects. *Eur. J. Neurosci.* 11:975–985. doi:10.1046/j.1460-9568.1999.00505.x

Cestèle, S., V. Yarov-Yarovoy, Y. Qu, F. Sampieri, T. Scheuer, and W.A. Catterall. 2006. Structure and function of the voltage sensor of sodium channels probed by a beta-scorpion toxin. *J. Biol. Chem.* 281:21332–21344. doi:10.1074/jbc.M603814200

Chakrapani, S., L.G. Cuello, D.M. Cortes, and E. Perozo. 2008. Structural dynamics of an isolated voltage-sensor domain in a lipid bilayer. *Structure.* 16:398–409. doi:10.1016/j.str.2007.12.015

Chanda, B., and F. Bezanilla. 2002. Tracking voltage-dependent conformational changes in skeletal muscle sodium channel during activation. *J. Gen. Physiol.* 120:629–645. doi:10.1085/jgp.20028679

Copel, C., N. Osorio, M. Crest, M. Gola, P. Delmas, and N. Clerc. 2009. Activation of neurokinin 3 receptor increases Na(v)1.9 current in enteric neurons. *J. Physiol.* 587:1461–1479. doi:10.1113/jphysiol.2009.169409

Coste, B., M. Crest, and P. Delmas. 2007. Pharmacological dissection and distribution of NaN/Nav1.9, T-type Ca^{2+} currents, and mechanically activated cation currents in different populations of DRG neurons. *J. Gen. Physiol.* 129:57–77. doi:10.1085/jgp.200609665

Cox, J.J., F. Reimann, A.K. Nicholas, G. Thornton, E. Roberts, K. Springell, G. Karbani, H. Jafri, J. Mannan, Y. Raashid, et al. 2006. An SCN9A channelopathy causes congenital inability to experience pain. *Nature.* 444:894–898. doi:10.1038/nature05413

Cummins, T.R., S.D. Dib-Hajj, J.A. Black, A.N. Akopian, J.N. Wood, and S.G. Waxman. 1999. A novel persistent tetrodotoxin-resistant sodium current in SNS-null and wild-type small primary sensory neurons. *J. Neurosci.* 19:RC43.

del Camino, D., M. Kanevsky, and G. Yellen. 2005. Status of the intracellular gate in the activated-not-open state of shaker K^+ channels. *J. Gen. Physiol.* 126:419–428. doi:10.1085/jgp.200509385

Dib-Hajj, S., J.A. Black, T.R. Cummins, and S.G. Waxman. 2002. NaN/Nav1.9: a sodium channel with unique properties. *Trends Neurosci.* 25:253–259. doi:10.1016/S0166-2236(02)02150-1

Dib-Hajj, S.D., T.R. Cummins, J.A. Black, and S.G. Waxman. 2010. Sodium channels in normal and pathological pain. *Annu. Rev. Neurosci.* 33:325–347. doi:10.1146/annurev-neuro-060909-153234

Fang, X., L. Djouhri, S. McMullan, C. Berry, S.G. Waxman, K. Okuse, and S.N. Lawson. 2006. Intense isolectin-B4 binding in rat dorsal root ganglion neurons distinguishes C-fiber nociceptors with broad action potentials and high Nav1.9 expression. *J. Neurosci.* 26:7281–7292. doi:10.1523/JNEUROSCI.1072-06.2006

Fertleman, C.R., M.D. Baker, K.A. Parker, S. Moffatt, F.V. Elmslie, B. Abrahamsen, J. Ostman, N. Klugbauer, J.N. Wood, R.M. Gardiner, and M. Rees. 2006. SCN9A mutations in paroxysmal extreme pain disorder: allelic variants underlie distinct channel defects and phenotypes. *Neuron.* 52:767–774. doi:10.1016/j.neuron.2006.10.006

Frech, G.C., A.M. VanDongen, G. Schuster, A.M. Brown, and R.H. Joho. 1989. A novel potassium channel with delayed rectifier properties isolated from rat brain by expression cloning. *Nature.* 340:642–645. doi:10.1038/340642a0

Garcia, M.L., M. Garcia-Calvo, P. Hidalgo, A. Lee, and R. MacKinnon. 1994. Purification and characterization of three inhibitors of voltage-dependent K+ channels from Leiurus quinquestriatus var. hebraeus venom. *Biochemistry.* 33:6834–6839. doi:10.1021/bi00188a012

Hille, B. 2001. Ion Channels of Excitable Membranes. Vol. 1. Third edition. Sinauer Associates, Inc., MA. 814 pp.

Horn, R., S. Ding, and H.J. Gruber. 2000. Immobilizing the moving parts of voltage-gated ion channels. *J. Gen. Physiol.* 116:461–476. doi:10.1085/jgp.116.3.461

Hoshi, T.W.N., W.N. Zagotta, and R.W. Aldrich. 1994. Shaker potassium channel gating. I: transitions near the open state. *J. Gen. Physiol.* 103:249–278. doi:10.1085/jgp.103.2.249

Isom, L.L.K.S., K.S. De Jongh, D.E. Patton, B.F. Reber, J. Offord, H. Charbonneau, K. Walsh, A.L. Goldin, and W.A. Catterall. 1992. Primary structure and functional expression of the beta 1 subunit of the rat brain sodium channel. *Science.* 256:839–842. doi:10.1126/science.1375395

Jiang, Y., A. Lee, J. Chen, V. Ruta, M. Cadene, B.T. Chait, and R. MacKinnon. 2003a. X-ray structure of a voltage-dependent K+ channel. *Nature.* 423:33–41. doi:10.1038/nature01580

Jiang, Y., V. Ruta, J. Chen, A. Lee, and R. MacKinnon. 2003b. The principle of gating charge movement in a voltage-dependent K+ channel. *Nature.* 423:42–48. doi:10.1038/nature01581

Jung, H.J., J.Y. Lee, S.H. Kim, Y.J. Eu, S.Y. Shin, M. Milescu, K.J. Swartz, and J.I. Kim. 2005. Solution structure and lipid membrane partitioning of VSTx1, an inhibitor of the KvAP potassium channel. *Biochemistry.* 44:6015–6023. doi:10.1021/bi0477034

Ledwell, J.L., and R.W. Aldrich. 1999. Mutations in the S4 region isolate the final voltage-dependent cooperative step in potassium channel activation. *J. Gen. Physiol.* 113:389–414. doi:10.1085/jgp.113.3.389

Lee, C.W., S. Kim, S.H. Roh, H. Endoh, Y. Kodera, T. Maeda, T. Kohno, J.M. Wang, K.J. Swartz, and J.I. Kim. 2004. Solution structure and functional characterization of SGTx1, a modifier of Kv2.1 channel gating. *Biochemistry.* 43:890–897. doi:10.1021/bi0353373

Leipold, E., S. Lu, D. Gordon, A. Hansel, and S.H. Heinemann. 2004. Combinatorial interaction of scorpion toxins Lqh-2, Lqh-3, and LqhalphaIT with sodium channel receptor sites-3. *Mol. Pharmacol.* 65:685–691. doi:10.1124/mol.65.3.685

Leo, S., R. D'Hooge, and T. Meert. 2010. Exploring the role of nociceptor-specific sodium channels in pain transmission using Nav1.8 and Nav1.9 knockout mice. *Behav. Brain Res.* 208:149–157. doi:10.1016/j.bbr.2009.11.023

Li-Smerin, Y., and K.J. Swartz. 2000. Localization and molecular determinants of the Hanatoxin receptors on the voltage-sensing domains of a K^+ channel. *J. Gen. Physiol.* 115:673–684. doi:10.1085/jgp.115.6.673

Long, S.B., X. Tao, E.B. Campbell, and R. MacKinnon. 2007. Atomic structure of a voltage-dependent K+ channel in a lipid membrane-like environment. *Nature.* 450:376–382. doi:10.1038/nature06265

Maingret, F., B. Coste, F. Padilla, N. Clerc, M. Crest, S.M. Korogod, and P. Delmas. 2008. Inflammatory mediators increase Nav1.9 current and excitability in nociceptors through a coincident detection mechanism. *J. Gen. Physiol.* 131:211–225. doi:10.1085/jgp.200709935

Marcotte, P., L.Q. Chen, R.G. Kallen, and M. Chahine. 1997. Effects of Tityus serrulatus scorpion toxin gamma on voltage-gated Na+ channels. *Circ. Res.* 80:363–369.

Martin, M.F., L.G. Garcia y Perez, M. el Ayeb, C. Kopeyan, G. Bechis, E. Jover, and H. Rochat. 1987a. Purification and chemical and biological characterizations of seven toxins from the Mexican scorpion, Centruroides suffusus suffusus. *J. Biol. Chem.* 262:4452–4459.

Martin, M.F., H. Rochat, P. Marchot, and P.E. Bougis. 1987b. Use of high performance liquid chromatography to demonstrate quantitative variation in components of venom from the scorpion Androctonus australis Hector. *Toxicon.* 25:569–573. doi:10.1016/0041-0101(87)90293-5

Maruyama, H., M. Yamamoto, T. Matsutomi, T. Zheng, Y. Nakata, J.N. Wood, and N. Ogata. 2004. Electrophysiological characterization of the tetrodotoxin-resistant Na+ channel, Na(v)1.9, in mouse dorsal root ganglion neurons. *Pflugers Arch.* 449:76–87. doi:10.1007/s00424-004-1315-0

McDonough, S.I., R.A. Lampe, R.A. Keith, and B.P. Bean. 1997. Voltage-dependent inhibition of N- and P-type calcium channels by the peptide toxin omega-grammotoxin-SIA. *Mol. Pharmacol.* 52:1095–1104.

Middleton, R.E., V.A. Warren, R.L. Kraus, J.C. Hwang, C.J. Liu, G. Dai, R.M. Brochu, M.G. Kohler, Y.D. Gao, V.M. Garsky, et al. 2002. Two tarantula peptides inhibit activation of multiple sodium channels. *Biochemistry.* 41:14734–14747. doi:10.1021/bi026546a

Milescu, M., F. Bosmans, S. Lee, A.A. Alabi, J.I. Kim, and K.J. Swartz. 2009. Interactions between lipids and voltage sensor paddles detected with tarantula toxins. *Nat. Struct. Mol. Biol.* 16:1080–1085. doi:10.1038/nsmb.1679

Nassar, M.A., L.C. Stirling, G. Forlani, M.D. Baker, E.A. Matthews, A.H. Dickenson, and J.N. Wood. 2004. Nociceptor-specific gene deletion reveals a major role for Nav1.7 (PN1) in acute and inflammatory pain. *Proc. Natl. Acad. Sci. USA.* 101:12706–12711. doi:10.1073/pnas.0404915101

Ostman, J.A., M.A. Nassar, J.N. Wood, and M.D. Baker. 2008. GTP up-regulated persistent Na+ current and enhanced nociceptor excitability require NaV1.9. *J. Physiol.* 586:1077–1087. doi:10.1113/jphysiol.2007.147942

Pathak, M., L. Kurtz, F. Tombola, and E. Isacoff. 2005. The cooperative voltage sensor motion that gates a potassium channel. *J. Gen. Physiol.* 125:57–69. doi:10.1085/jgp.200409197

Phillips, L.R., M. Milescu, Y. Li-Smerin, J.A. Mindell, J.I. Kim, and K.J. Swartz. 2005. Voltage-sensor activation with a tarantula toxin as cargo. *Nature.* 436:857–860. doi:10.1038/nature03873

Priest, B.T., B.A. Murphy, J.A. Lindia, C. Diaz, C. Abbadie, A.M. Ritter, P. Liberator, L.M. Iyer, S.F. Kash, M.G. Kohler, et al. 2005. Contribution of the tetrodotoxin-resistant voltage-gated sodium channel NaV1.9 to sensory transmission and nociceptive behavior. *Proc. Natl. Acad. Sci. USA.* 102:9382–9387. doi:10.1073/pnas.0501549102

Priest, B.T., K.M. Blumenthal, J.J. Smith, V.A. Warren, and M.M. Smith. 2007. ProTx-I and ProTx-II: gating modifiers of voltage-gated sodium channels. *Toxicon.* 49:194–201. doi:10.1016/j.toxicon.2006.09.014

Rogers, J.C., Y. Qu, T.N. Tanada, T. Scheuer, and W.A. Catterall. 1996. Molecular determinants of high affinity binding of alpha-scorpion toxin and sea anemone toxin in the S3-S4 extracellular loop in domain IV of the Na+ channel alpha subunit. *J. Biol. Chem.* 271:15950–15962. doi:10.1074/jbc.271.27.15950

Rush, A.M., and S.G. Waxman. 2004. PGE2 increases the tetrodotoxin-resistant Nav1.9 sodium current in mouse DRG neurons via G-proteins. *Brain Res.* 1023:264–271. doi:10.1016/j.brainres.2004.07.042

Ruta, V., J. Chen, and R. MacKinnon. 2005. Calibrated measurement of gating-charge arginine displacement in the KvAP voltage-dependent K+ channel. *Cell.* 123:463–475. doi:10.1016/j.cell.2005.08.041

Schoppa, N.E., and F.J. Sigworth. 1998a. Activation of *Shaker* potassium channels. I. Characterization of voltage-dependent transitions. *J. Gen. Physiol.* 111:271–294. doi:10.1085/jgp.111.2.271

Schoppa, N.E., and F.J. Sigworth. 1998b. Activation of *Shaker* potassium channels. II. Kinetics of the V2 mutant channel. *J. Gen. Physiol.* 111:295–311. doi:10.1085/jgp.111.2.295

Schoppa, N.E., and F.J. Sigworth. 1998c. Activation of *Shaker* potassium channels. III. An activation gating model for wild-type and V2 mutant channels. *J. Gen. Physiol.* 111:313–342. doi:10.1085/jgp.111.2.313

Seoh, S.A., D. Sigg, D.M. Papazian, and F. Bezanilla. 1996. Voltage-sensing residues in the S2 and S4 segments of the Shaker K+ channel. *Neuron.* 16:1159–1167. doi:10.1016/S0896-6273(00)80142-7

Sheets, M.F., J.W. Kyle, R.G. Kallen, and D.A. Hanck. 1999. The Na channel voltage sensor associated with inactivation is localized to

the external charged residues of domain IV, S4. *Biophys. J.* 77:747–757. doi:10.1016/S0006-3495(99)76929-8

Sivilotti, L., K. Okuse, A.N. Akopian, S. Moss, and J.N. Wood. 1997. A single serine residue confers tetrodotoxin insensitivity on the rat sensory-neuron-specific sodium channel SNS. *FEBS Lett.* 409:49–52. doi:10.1016/S0014-5793(97)00479-1

Smith-Maxwell, C.J., J.L. Ledwell, and R.W. Aldrich. 1998a. Role of the S4 in cooperativity of voltage-dependent potassium channel activation. *J. Gen. Physiol.* 111:399–420. doi:10.1085/jgp.111.3.399

Smith-Maxwell, C.J., J.L. Ledwell, and R.W. Aldrich. 1998b. Uncharged S4 residues and cooperativity in voltage-dependent potassium channel activation. *J. Gen. Physiol.* 111:421–439. doi:10.1085/jgp.111.3.421

Stefani, E., L. Toro, E. Perozo, and F. Bezanilla. 1994. Gating of Shaker K+ channels: I. Ionic and gating currents. *Biophys. J.* 66:996–1010. doi:10.1016/S0006-3495(94)80881-1

Stühmer, W., J.P. Ruppersberg, K.H. Schröter, B. Sakmann, M. Stocker, K.P. Giese, A. Perschke, A. Baumann, and O. Pongs. 1989. Molecular basis of functional diversity of voltage-gated potassium channels in mammalian brain. *EMBO J.* 8:3235–3244.

Sukhareva, M., D.H. Hackos, and K.J. Swartz. 2003. Constitutive activation of the Shaker Kv channel. *J. Gen. Physiol.* 122:541–556. doi:10.1085/jgp.200308905

Swartz, K.J. 2007. Tarantula toxins interacting with voltage sensors in potassium channels. *Toxicon.* 49:213–230. doi:10.1016/j.toxicon.2006.09.024

Swartz, K.J. 2008. Sensing voltage across lipid membranes. *Nature.* 456:891–897. doi:10.1038/nature07620

Swartz, K.J., and R. MacKinnon. 1995. An inhibitor of the Kv2.1 potassium channel isolated from the venom of a Chilean tarantula. *Neuron.* 15:941–949. doi:10.1016/0896-6273(95)90184-1

Swartz, K.J., and R. MacKinnon. 1997a. Hanatoxin modifies the gating of a voltage-dependent K+ channel through multiple binding sites. *Neuron.* 18:665–673. doi:10.1016/S0896-6273(00)80306-2

Swartz, K.J., and R. MacKinnon. 1997b. Mapping the receptor site for hanatoxin, a gating modifier of voltage-dependent K+ channels. *Neuron.* 18:675–682. doi:10.1016/S0896-6273(00)80307-4

Zagotta, W.N., T. Hoshi, and R.W. Aldrich. 1994a. Shaker potassium channel gating. III: evaluation of kinetic models for activation. *J. Gen. Physiol.* 103:321–362. doi:10.1085/jgp.103.2.321

Zagotta, W.N., T. Hoshi, J. Dittman, and R.W. Aldrich. 1994b. Shaker potassium channel gating. II: transitions in the activation pathway. *J. Gen. Physiol.* 103:279–319. doi:10.1085/jgp.103.2.279

Zimmermann, K., A. Leffler, A. Babes, C.M. Cendan, R.W. Carr, J. Kobayashi, C. Nau, J.N. Wood, and P.W. Reeh. 2007. Sensory neuron sodium channel Nav1.8 is essential for pain at low temperatures. *Nature.* 447:856–859. doi:10.1038/nature05880